Journal of Power Sources 244 (2013) 287–293

Contents lists available at SciVerse ScienceDirect

Journal of Power Sources

journal homepage: www.elsevier.com/locate/jpowsour

# High performance composite solid polymer electrolyte systems for electrochemical cells

G.M. Wu [a,b,*], S.J. Lin [b,c], C.C. Yang [c]

[a] Dept. of Materials Science and Engineering, University of California, Los Angeles, CA 90095, USA
[b] Institute of Electro-Optical Engineering, Dept. of Chemical and Materials Engineering, Chang Gung University, Taoyuan 333, Taiwan
[c] Dept. of Chemical Engineering, Ming Chi University of Technology, Taipei 243, Taiwan

## HIGHLIGHTS

- New composite solid polymer electrolytes were developed to exhibit both high ionic conductivity and high mechanical strength.
- The cyclic voltammetry analysis indicated excellent electrochemical stability.
- The solid-state fuel cells showed excellent discharge capacity of 1506 mAh.
- The anode utilization was very good at 95.7%.
- The battery power density has been achieved at 91 mW $cm^{-2}$.

## ARTICLE INFO

*Article history:*
Received 17 November 2012
Received in revised form
30 December 2012
Accepted 8 January 2013
Available online 16 January 2013

*Keywords:*
Composite
Solid polymer electrolyte
Battery discharge capacity
Power density

## ABSTRACT

We report high performance composite solid polymer electrolytes for electrochemical cells with comprehensive properties in high mechanical strength and high ionic conductivity. The composite electrolytes consist of porous non-woven polymer filament substrates that are impregnated with high ion-conducting materials. To insure structural integrity, the non-woven polypropylene/polyethylene core–shell substrates are sulfonated to activate the surface. The high ion-conducting materials are prepared from poly(vinyl alcohol) with the incorporation of acrylic acid monomer and cross-linking agent. The results show well-balanced physical and electrochemical characteristics that warrant excellent battery discharge capacity and cell power density. The room temperature ionic conductivity is high at 0.16–0.21 S $cm^{-1}$, and the activation energy is low at 0.5 kJ $mol^{-1}$. The mechanical strength is improved to 12 MPa with good elongation at 58–62%. The anionic transport numbers ($t^-$) are in the range of 0.93–0.99 in 1 M KOH, 0.91–0.97 in 1 M NaOH, and 0.83–0.91 in 1 M LiOH, respectively. The cyclic voltammetric study indicates good stability with symmetric curves between the cathodic and anodic peaks. The fully solid-state metal–air fuel cells exhibit excellent discharge capacity of 1506 mAh and high anode utilization of 95.7%. The power density is achieved at 91 mW $cm^{-2}$.



## 1. Introduction

The demand for high performance energy conversion materials/devices has been raised substantially due to the increased concerns in natural resources deficiency and environmental protection. The successful development of high efficient and clean electrochemical devices can help to reduce the greenhouse effect and the contamination in our environment. Several primary and secondary battery systems have been introduced to the consumers in the last decade due to the rapid market growth in portable electronic devices such as notebook computers, mobile phones, personal digital assistants, digital cameras and video camcorders. These include Li-ion batteries, Ni-MH (metal hydride) batteries and Zn-air batteries [1–5]. Among the major components of a high quality battery, a polymer electrolyte should exhibit sufficient ionic conductivity while providing long-life cell performance [6,7]. The key factors for a successful electrolyte include high ionic conductivity, sufficient mechanical strength, good chemical/environmental stability, and acceptable production cost [8–10].

Several endeavors have been carried out to achieve the comprehensive performances [11–13]. Idris et al. prepared microporous poly(vinylidene fluoride)/poly(methyl methacrylate) gel polymer

* Corresponding author. Institute of Electro-Optical Engineering, Dept. of Chemical and Materials Engineering, Chang Gung University, Taoyuan 333, Taiwan. Tel.: +886 3 2118800; fax: +886 3 2118700.
*E-mail address:* wu@mail.cgu.edu.tw (G.M. Wu).

0378-7753/$ – see front matter © 2013 Elsevier B.V. All rights reserved.
http://dx.doi.org/10.1016/j.jpowsour.2013.01.044

electrolytes by phase-separation method. The maximum ionic conductivity at room temperature was $1.21 \times 10^{-3}$ S cm$^{-1}$ [14]. Park et al. used close-packed poly(methyl methacrylate) nanoparticle arrays to coat polyethylene separators and achieved favorable liquid electrolyte wettability [12]. Liao et al. doped nano–$Al_2O_3$ in the polyethylene-supported poly(methyl methacrylate-vinyl acetate)-co-poly(ethylene glycol) diacrylate based gel polymer electrolytes. Their ionic conductivity was improved to $3.8 \times 10^{-3}$ S cm$^{-1}$ and the mechanical strength and the decomposition temperature were both increased [13]. Merle et al. evaluated cross-linked poly(vinyl alcohol) and reported a maximum power density of 72 mW cm$^{-2}$ at 0.34 V [15]. In addition, composite polymer non-woven membrane electrolytes have been prepared by electrospinning to enhance battery cycle performance and initial discharge properties [16,17]. On the other hand, the successfully developed sulfonated polymers, such as Nafion, have high conductivity and could be employed in fuel cells. The expensive cost certainly put some limitation on their popularity [18]. However, sulfonation treatments increase polymer surface hydrophilicity. The polymer surface can be activated for better bonding with a secondary material due to higher interfacial shear strength [19,20]. The objective of this study has been therefore to develop high performance composite solid polymer electrolytes with improved reliability and processibility. High ionic conductivity and high electrochemical cell power density, in conjunction with good mechanical strength and thermal stability, are inevitably demanded by the different battery systems.

The composite solid polymer electrolytes are consisted of porous non-woven membrane substrates that become impregnated with high ion-conducting polymer materials. The polypropylene/polyethylene (PP/PE) core–shell substrates were sulfonated by concentrated sulfuric acid to activate the polymer surface. The sulfonated substrates (s-PP/PE) were then impregnated with anionic-conducting polymer formulation for electrochemical cell evaluation. Poly(vinyl alcohol) (PVA) showed excellent hydrophilicity and the alkaline PVA-based polymer includes a water-swollen matrix and alkali electrolyte solution. The hydroxyl ion transport takes place in the electrolyte by the means of both water vehicle and tunneling. The incorporation of poly(acrylic acid) (PAA) with cross-linking agent provides a semi-interpenetrating network with PVA. A decrease in polymer crystallinity can improve chain flexibility for more efficient ionic transport in the amorphous region. The physical and electrochemical characteristics of the composite solid polymer electrolytes have been carefully investigated. Differential scanning calorimeter (DSC) and thermogravimetric analysis (TGA) were employed to analyze the thermal properties. X-ray diffraction (XRD) was used to study the crystalline structure, and scanning electron microscopy (SEM) revealed the morphology. The ionic conductivity was measured by AC impedance spectroscopy. The mechanical strength and elongation behavior were tested on a tensile stress-strain testing machine. Metal-fuel cells were assembled with a zinc gel anode and a porous carbon air diffusion cathode. The electrochemical stability was quantified by cyclic voltammetry analysis. Some cell samples were also prepared for the galvanostatic discharge study.

## 2. Experimental

The non-woven polypropylene/polyethylene was received from Coin Nanotech. The flat sheet had a nominal thickness of 0.2 mm and porosity about 70%. The average area weight was 60 g m$^{-2}$. It was sulfonated by 98 wt-% sulfuric acid solution at 90 °C for 72 h. After the reaction, the substrates were repeatedly rinsed in D.I. water under ultrasonic agitation, until the water reached pH of 6.5–7.0. The completely rinsed samples were dried at 105 °C for 5 h.

PVA (M.W. 75,000–80,000, Chang Chung Chemicals), acrylic acid monomer (Aldrich) and KOH (Merck) were used as received. The designated weight ratios of acrylic acid monomer (10:3 to 10:7.5 with respect to PVA) and 1 wt-% cross-linker (triallylamine, Aldrich) were dissolved in D.I. water with agitation for about 12 h at 60 °C. The monomer solution was added with 75 mol-% KOH. The mixture was blended until completely homogeneous, and the s-PP/PE substrates were added. The appropriate weight percent (10 wt-% by AA monomer) of initiator (ammonium persulfate, $(NH_4)_2S_2O_8$, Aldrich) was finally added into the highly viscous mixture for free-radical polymerization under stirring at 90 °C for 6 h. The s-PP/PE substrates were impregnated with the viscous polymer solution. They could be then poured onto a poly(tetrafluoro ethylene) (PTFE) plate, and the excess water solvent was evaporated slowly at 80 °C in a vacuum oven.

The free-standing composite polymer electrolytes were further immersed in 32 wt-% KOH solution for 24 h. The conductivity measurements were carried out by AC impedance method. The blocking electrodes had contact area of 0.785 cm$^2$. The AC impedance measurements were carried out using an AutoLab from Eco Chemi with a computer program. The frequency range from 100 Hz to 100 kHz at an excitation signal of 10 mV was recorded. The AC impedance was measured from 30 °C to 80 °C. In addition, the cyclic voltammetry measurements for the Zn|s-PP/PE/PVA/PAA|Zn systems were conducted by Autolab PGSTAT 30 equipment and a computer program GPES.

The DSC thermal analysis was employed using a Perkin Elmer Pyris 7 DSC system. The samples were at first heated to 105 °C for dehydration, and then scanned from 25 °C to 275 °C, at a heating rate of 10 °C min$^{-1}$ in $N_2$ atmosphere. TGA thermal analysis used Perkin Elmer Pyris 7 TGA system. The measurements were made from 25 °C to 550 °C, also at a heating rate of 10 °C min$^{-1}$ under $N_2$ atmosphere. The crystalline structure was examined by Philips X'Pert X-ray diffractometer (XRD) using Cu K$\alpha$ irradiation of wavelength $\lambda$ 0.154 nm. The surface morphology and the cross-section microstructure could be revealed by Hitachi S-2600H scanning electron microscope. The mechanical strength was evaluated from the stress–strain curves on Instron model 5544 universal instrument. A mini-tensile bar based on ASTM with the gauge length of 2.94 cm and width 0.45 cm was pulled at a cross-head speed of 20 cm min$^{-1}$.

The zinc powder gel was prepared by weighing 1% $In(Ac)_3$ inhibitor and adding in 32 wt-% KOH solution under agitation. It was mixed with 67 wt-% zinc powders (UM) into the gel solution in an ultrasonic oscillator for about 1 h. The purity of zinc was 99.995 wt-% and the powder size of 100–200 μm. An additional 1 wt-% polyacrylic polymer gelling agent (Carbopol 940) was finally added to form a highly viscous gel, and the zinc gel anode was thus obtained. The porous carbon air cathode was prepared by taking proper amounts of Triton-X, PTFE-30 and $H_2O$, mixing them uniformly, and adding designated AB50 carbon powder to the mixture. The mixture was then dried at 120 °C to remove $H_2O$. The dried mixture was ground and coated uniformly on a nickel screen, before being sintered in a thermal press for about 0.5 h under 10 MPa at 300 °C. The active layer of the air electrode was prepared by spraying a mixture of 15 wt-% PTFE-30 binder, 10 wt-% $KMnO_4$/$MnO_2$ (2:1) catalyst, 60 wt-% Vulcan XC-72R carbon powder, isopropanol, methanol and $H_2O$ onto the gas-diffusion layer. The air electrode was finally sintered for about 0.5 h at 360 °C at 8 MPa. The thickness of the air cathode electrode was about 0.5 mm. The solid-state zinc-air battery, with zinc gel anode, porous air cathode, and s-PP/PE/PVA/PAA composite polymer electrolyte, could be assembled in $2 \times 3$ cm$^2$ cell for electrochemical evaluation. The characteristics were measured with BAT778 constant current charge/discharge unit at room temperature.

## 3. Results and discussion

### 3.1. Microstructures

The X-ray diffraction scan curves of the composite samples are shown in Fig. 1. There are five distinct crystalline peaks from the s-PP/PE semi-crystalline sheet. The first three peaks at 2θ angle of 14.0°, 16.8°, 18.4° are from the polypropylene crystalline structure, and the other two peaks at 21.6° and 24.0° are from polyethylene. The peak intensity was reduced while the PAA composition ratio was increased. This suggested a lower degree of crystallinity from the good binding between the s-PP/PE substrates and the PVA/PAA polymers. The composite system has become more amorphous and could enhance the ionic conductivity due to the flexible local chain segmental motion in the polymer matrix. Fig. 2 presents the SEM micrographs of the composite system prepared from non-sulfonation PP/PE and well-sulfonated s-PP/PE substrates. The polymer composition has been PVA:PAA = 10:5 in both samples. The cross-section picture shows an enhanced binding quality between the polymer matrix and the substrate fiber when the sulfonation treatment time was increased to 72 h. This was attributed to the improvement in the hydrophilicity of the polymer system, and no phase separation was discernible. The fractured surface appears more brittle. On the other hand, the substrate fiber is only partially covered by the polymer matrix when no sulfonation treatment was taken. Voids are also clearly observed.

### 3.2. Mechanical properties

The stress-strain test results for the composites are summarized in Table 1. The s-PP/PE substrates exhibited a tensile strength of 10.75 MPa with 34% elongation. In general, the composite s-PP/PE/PVA/PAA system increased the thickness and elongation-at-break. When the composition ratio was chosen at PVA:PAA = 10:3, the mechanical strength was increased to 12.15 MPa and the ductility was improved to 62% elongation. The mechanical strength is comparable to nanoparticle-doped diacrylate based gel polymer electrolytes, but the ionic conductivity is much higher [13]. The chain extension and cross-linking reaction increased bonding quality and thus enhanced the composite membrane strength and elongation. However, when the PAA amount was increased (ratio 10:7.5), the mechanical strength could be lowered to 7.23 MPa and the elongation slightly reduced to 56%. Although higher PAA content provided more enhanced electrolyte absorption and ionic conducting characteristics, the weaker structure nature of PAA could result in declined membrane strength. The decreased crystallinity with increasing PAA content also reduced the composites' tensile strength. The amount of PAA thus needs to be carefully designed for optimization. Fortunately, the elongation data did not fall as much as the strength results when the PVA:PAA was changed to 10:7.5. High plasticity is beneficial for electrolyte processibility, and the composites can be easily manufactured for batteries in various sizes and shapes.

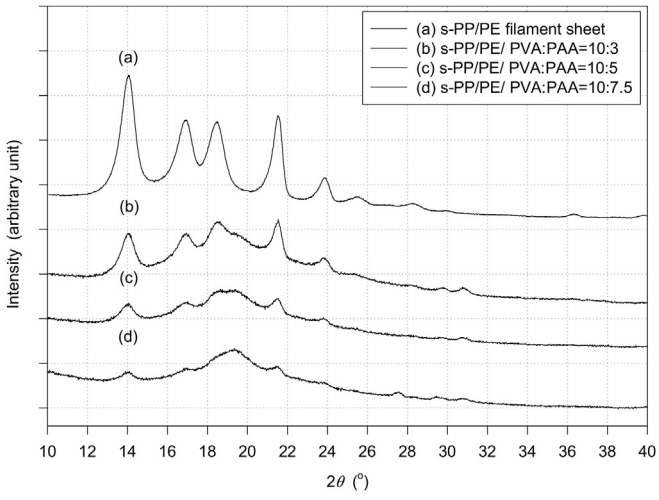


**Fig. 1.** XRD scan curves for s-PP/PE/PVA/PAA composites at the various composition ratios.

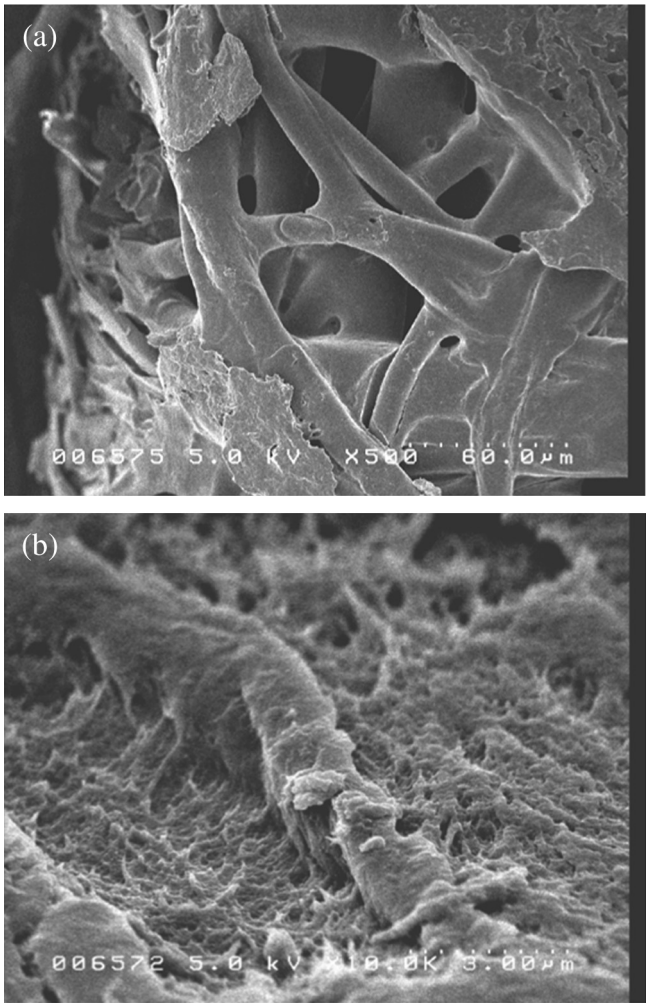


**Fig. 2.** SEM micrographs of the composite samples prepared from (a) non-sulfonation PP/PE substrate and (b) well-sulfonated 72 h s-PP/PE substrate.

### 3.3. Thermal analysis

The DSC thermographs for the composites with different composition ratios are displayed in Fig. 3. The curve from s-PP/PE has

**Table 1**
Mechanical properties of the composites at room temperature.

| Polymer sample | Thickness (mm) | Width (mm) | Strength (MPa) | Elongation (%) |
|---|---|---|---|---|
| s-PP/PE | 0.20 | 10 | 10.75 | 34 |
| s-PP/PE/PVA:PAA (10:3) | 0.52 | 10 | 12.15 | 62 |
| s-PP/PE/PVA:PAA (10:5) | 0.55 | 10 | 11.89 | 58 |
| s-PP/PE/PVA:PAA (10:7.5) | 0.55 | 10 | 7.23 | 56 |

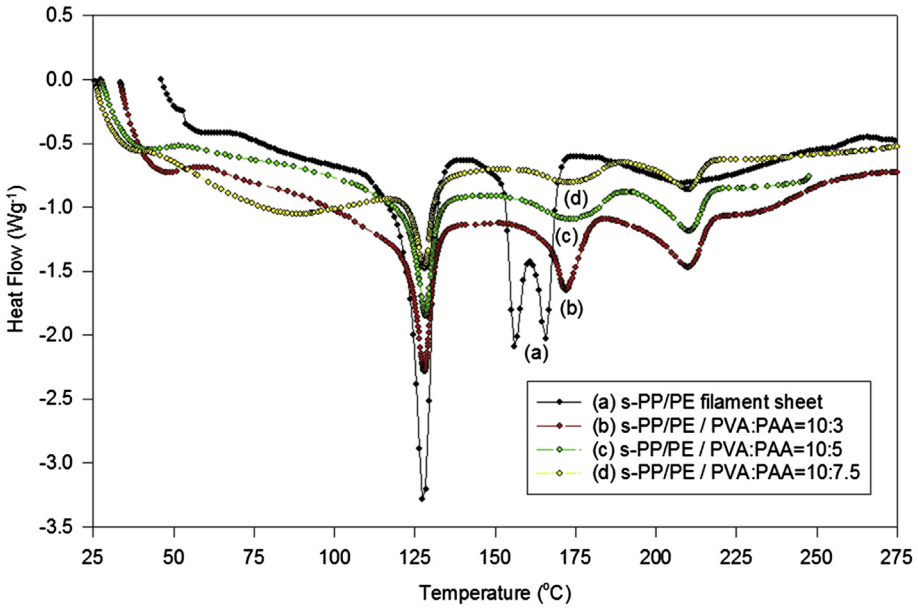


**Fig. 3.** DSC scans for the composites.

three endothermic peaks. It is noted that the $T_m$ of polyethylene and polypropylene are 130 °C and 160 °C [21]. The peak at 129 °C corresponds to the melting of polyethylene, while the two higher melting peaks at 158 °C and 168 °C are from polypropylene. A duplication of melting peaks was thus found for polypropylene in our polymer sample. This was a characteristic feature of polymers while the exothermic re-crystallization was superimposed with the endothermic melting process. In addition, the integrated area under the melting peaks has become smaller when the PAA composition ratio was increased. The higher melting peaks at 210–215 °C are from PVA polymer. The lower melting peak integrated area indicated a structural change from a more crystalline phase to an amorphous phase.

The TGA thermographs for the composites are given in Fig. 4. The curves exhibit multiple step degradation. The first region is nominally from the loss of free water in the polymer matrix at the temperature range below 150 °C. The weight loss for the PVA/PAA composition ratio of 10:5 sample in the temperature range of 310–370 °C is mainly from the decomposition of PAA. The onset decomposition temperature for PVA starts at around 410–430 °C. The s-PP/PE substrate exhibits one-step degradation with a peak loss at 478 °C. At this temperature range, the composite become severely degraded. On the other hand, the weight loss degradation can be slightly relieved when compared with the s-PP/PE alone. Nevertheless, the composite samples have been relatively stable in the temperature range of 100–280 °C.

### 3.4. Ionic conductivity

Fig. 5 provides the Nyquist plots from AC impedance analysis for the alkaline composite electrolytes. The AC impedance spectra show two well-defined regions. At the high frequency range, it is

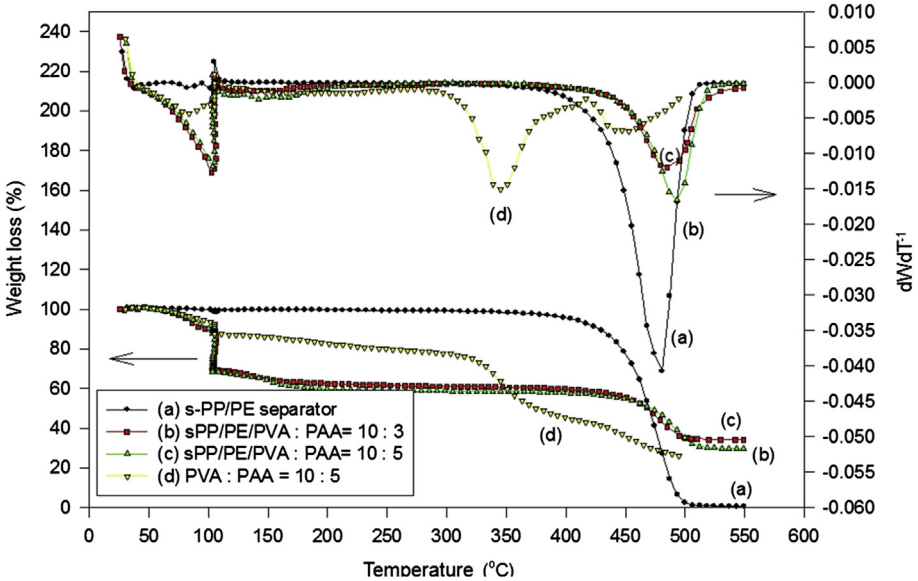


**Fig. 4.** TGA thermographs for the composites.

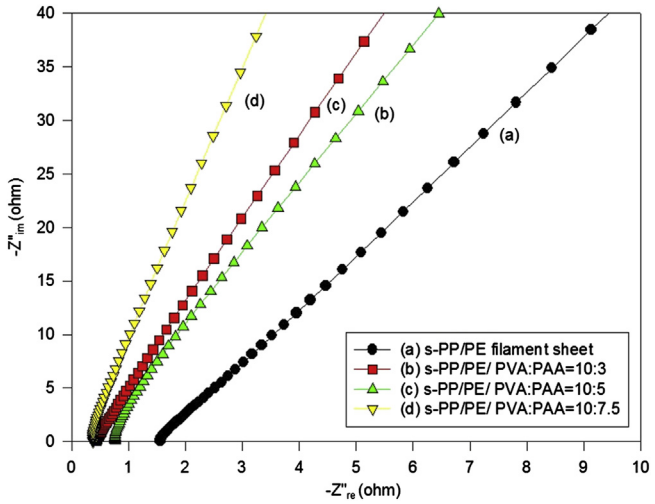


**Fig. 5.** AC impedance spectra for the composite electrolytes at room temperature.

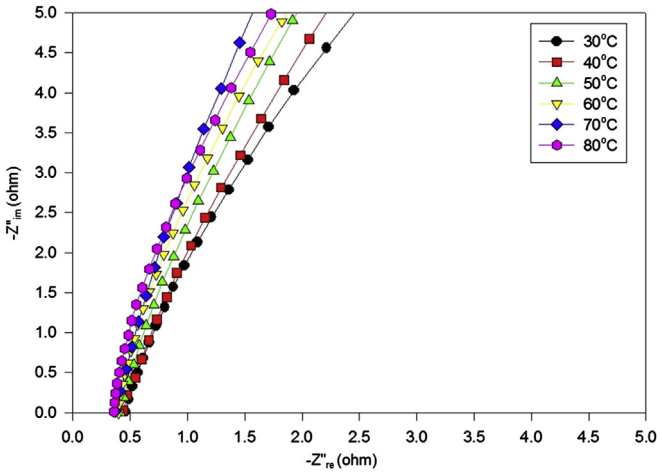


**Fig. 6.** Effects of temperature on the AC impedance spectra for the composite electrolytes. The PVA/PAA polymer composition ratio has been 10:5.

related to the ionic conduction process in the bulk of the polymer electrolyte. At the low frequency range, a straight line parallel to the imaginary axis has been found, which is attributed to the effect of blocking electrode. The analysis of the spectra yields information about the bulk resistance ($R_b$). It is then calculated from the intercept at the high frequency side on the $Z_{re}$ axis. The $R_b$ value is converted into the ionic conductivity by the equation $\sigma = l\,R_b^{-1}\,A^{-1}$, where $l$ is the thickness (cm) of the composite electrolytes, A is the area of the blocking electrode ($cm^2$), and $R_b$ is the bulk resistance (ohm).

The experimental values of $R_b$ for the composites have been in the range of 0.37–0.78 Ω, depending on the PVA/PAA ratio. The highest room temperature ionic conductivity value was 0.21 S $cm^{-1}$ when the polymer composition ratio was 10:7.5. This indicated a more than 10-fold increase from that of the s-PP/PE. Table 2 lists the ionic conductivity data from the various samples. They are significantly higher than the conductivity properties of gel polymer electrolytes [12,14] and polyacrylonitrile non-woven membranes [16]. The semi-interpenetrating network structure formed by free-radical polymerization provided high hydrophilicity and well dispersed amorphous region to contain alkaline electrolytes. This increased the ionic transport among polymer chains. According to the conductivity measurement results, the higher the PAA content, the higher the ionic conductivity was obtained. In fact, both proton and hydroxide conducting electrolytes can be designed from this composite structure. On the other hand, the effects of temperature on the AC impedance spectra are shown in Fig. 6 for the alkaline composite electrolyte with PVA/PAA ratio of 10:5. It has been clearly evidenced that the $R_b$ value was decreased with the elevated temperature. The composite could thus exhibit higher ionic conductivity at the higher temperature range. In addition, the temperature dependence of the ionic conductivity is of the Arrhenius type. The log($\sigma$) *vs.* 1/T plots are provided in Fig. 7. We can extract the activation energy ($E_a$) information from the slope of Arrhenius plot by following the equation $\sigma = \sigma_o \times \exp(-E_a\,R^{-1}\,T^{-1})$. The $E_a$ value for the alkaline composite electrolytes have been 0.5 kJ $mol^{-1}$ and 0.8 kJ $mol^{-1}$, with respect to PVA/PAA ratio of 10:3 and 10:5. It was also noted to be significantly lower than that of the pure PVA/PAA = 10:5 polymer electrolyte, which was 1.2 kJ $mol^{-1}$. The composite polymer electrolytes are relatively more stable.

**Table 2**
Electrical properties of the composite electrolytes at room temperature.

| Polymer electrolytes | Thickness (cm) | Resistance (ohm) | Conductivity (S $cm^{-1}$) |
|---|---|---|---|
| s-PP/PE | 0.020 | 1.56 | 0.016 |
| s-PP/PE/PVA:PAA (10:3) | 0.055 | 0.78 | 0.090 |
| s-PP/PE/PVA:PAA (10:5) | 0.057 | 0.44 | 0.165 |
| s-PP/PE/PVA:PAA (10:7.5) | 0.061 | 0.37 | 0.210 |

### 3.5. Cyclic voltammetry analysis

For practical battery applications, it requires the electrolytes not only to have high ionic conductivity but also high electrochemical stability. In cyclic voltammetric study, the sweep potential was firstly scanned in the positive-going direction and then reversed. Fig. 8 shows the cyclic voltammograms for the s-PP/PE/PVA/PAA composite samples. The cyclic sweeping range is between −0.50 V and +0.50 V, with a scan rate of 10 mV $s^{-1}$ in the Zn|composite|Zn cell system. It has been evidenced that the cyclic voltammograms at the 3rd cycle for each composite could be seen with symmetric curves. The cathodic and anodic peaks between $E_{catho} = -0.1$ V and $E_{ano} = 0.1$ V were still symmetrical when the PVA/PAA ratio was varied from 10:3 to 10:7.5. In addition, it was noted that the higher

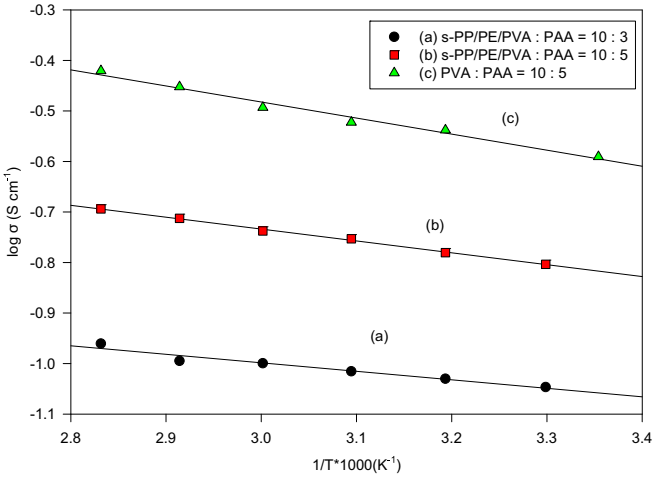


**Fig. 7.** Arrhenius plots for the s-PP/PE/PVA/PAA composites.

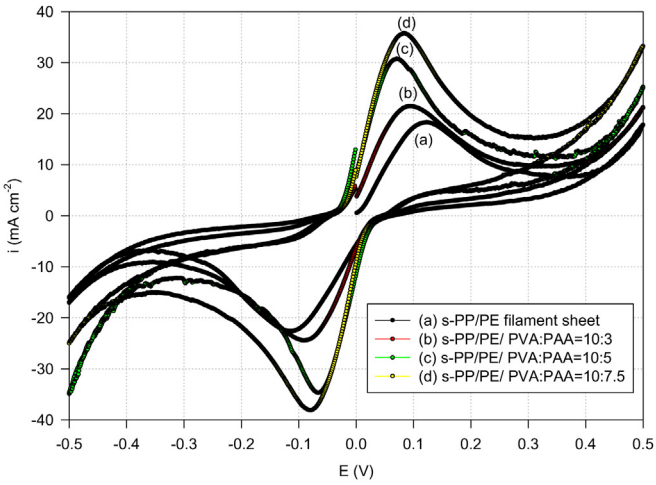


**Fig. 8.** The cyclic voltammograms for the Zn|composite|Zn cells at room temperature. The scan rate is 10 mV $s^{-1}$, and the 3rd sweeping cycles are shown.

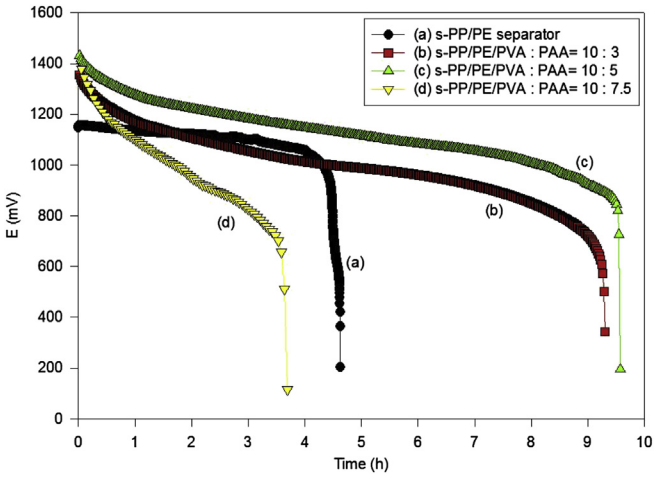


**Fig. 10.** Discharge curves for the Zn-air cells at C/10 discharge rate at room temperature.

the PAA ratio, the higher the reduction and oxidation current density. Finally, the results indicated that the alkaline composite electrolytes have excellent electrochemical stability.

### 3.6. Ionic transport properties

The ionic transport data of the composite electrolytes are provided in Fig. 9 at room temperature. The ionic transport numbers ($t^-$) were examined as functions of polymer composition and selected alkali metal salts. For the composites, the $t^-$ values are in the range of 0.93–0.99 in 1 M KOH solution, 0.91–0.97 in 1 M NaOH solution, and 0.83–0.91 in 1 M LiOH solution. On the other hand, for the s-PP/PE, the $t^-$ are much lower at 0.86 in 1 M KOH solution, 0.82 in 1 M NaOH solution and 0.8 in 1 M LiOH solution. The results supported that the s-PP/PE/PVA/PAA composites would enhance the ion transport capability in the polymers, which was in accordance with the trend in ionic conductivity analysis.

### 3.7. Electrochemical performance of metal fuel cells

The discharge curves of the solid-state metal fuel cells with the composite electrolytes at C/10 discharge rate at room temperature

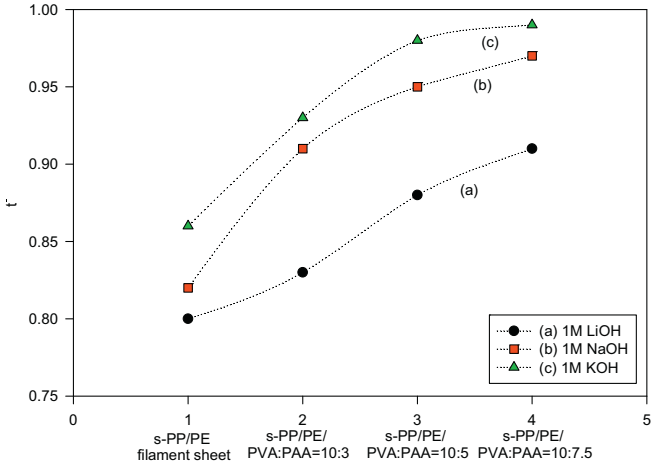


**Fig. 9.** Effects of different metal salts on the ionic transport numbers ($t^-$) for the composites at room temperature.

**Table 3**
The electrochemical analysis results for the metal-air cells at C/10 discharge rate. The cell dimension has been 2 cm × 3 cm, tested at 25 °C.

| Property | s-PP/PE | s-PP/PE/ PVA:PAA (10:3) | s-PP/PE/ PVA:PAA (10:5) | s-PP/PE/ PVA:PAA (10:7.5) |
|---|---|---|---|---|
| Theo. capacity (mAh) | 1574 | 1574 | 1574 | 1574 |
| Discharge current (mA) | 150 | 150 | 150 | 150 |
| Discharge time (h) | 4.63 | 93.08 | 95.71 | 36.95 |
| Real capacity (mAh) | 728 | 1465 | 1506 | 581 |
| Anode utilization (%) | 46.3 | 93.1 | 95.7 | 37.0 |

are shown in Fig. 10. The electrochemical testing results of the Zn–air cells are also summarized in Table 3. In this study, the gel anode had a zinc power capacity of 820 mAh $g^{-1}$ [22], and the experimental battery theoretical capacity was designed at 1574 mAh. The solid-state cell with the s-PP/PE has the lower discharge capacity of 728 mAh and the lower calculated Zn anode utilization of 46.3%. This suggested that, during the cell discharge process, the expansion of zinc anode and the produce of zincate could penetrate through the porous s-PP/PE to air cathode. The discharge time was thus only 4.63 h. However, with the new composite electrolytes (PVA/PAA = 10:5), the solid-state battery cells exhibited the highest

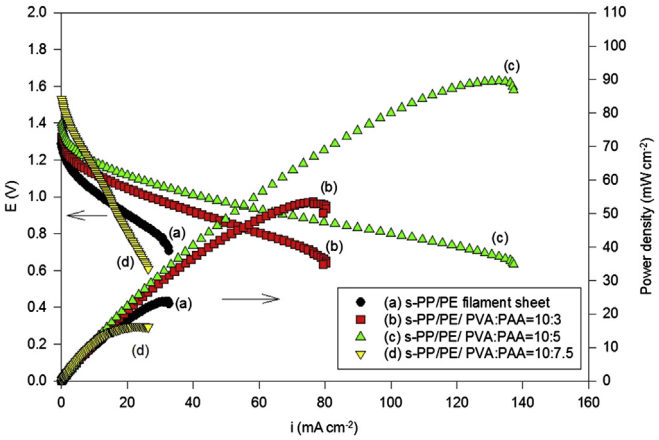


**Fig. 11.** Cell potential and the corresponding power density curves of the solid-state composite batteries as functions of the discharge current density.

discharge capacity of 1506 mAh and the highest zinc anode utilization of 95.7%. The uniform morphology in the composite has effectively impeded the zincate penetration and thus extended the cell discharge life. It was also noted that the higher PAA content cell (PVA/PAA = 10:7.5) had a very low discharge capacity. After the cell discharge tests, we dissembled the cells and observed problem in dimension stability. The high PAA content sample absorbed too much electrolyte and became curled, which in term curtailed the cell discharge life.

Fig. 11 displays the cell potential ($E$) of the electrochemical cells as a function of the discharge current density. The corresponding power density curves are also included. It was found that the batteries with the composition ratio of PVA/PAA = 10:5 would have the highest power density of 91 mW $cm^{-2}$. This shows some improvement from cross-linked poly(vinyl alcohol) [10,15]. Therefore, the solid-state cells with the appropriate composite electrolytes exhibited excellent electrochemical property and cell performance.

## 4. Conclusion

Comprehensive performance composite polymer electrolyte battery cells have been successfully prepared. They showed the advantages in both high mechanical strength and high ionic conductivity. The optimum constituents for the composite electrolyte were composed of a 72-h-sulfonation treated PP/PE porous substrate, and poly(vinyl alcohol) and poly(acrylic acid), particularly at the composition ratio of 10:5. The composite exhibited a high ionic conductivity of 0.165 S $cm^{-1}$, and the anionic transport number could reach 0.99 in 1 M KOH. The mechanical tensile strength was good at 12.15 MPa. The composite showed low crystallinity and had uniform morphology. In addition, the composite maintained very good thermal stability. The composite electrolytes prolonged the cell discharge time and elevated the cell utilization to nearly 96%, and exhibited the highest battery power density of 91 mW $cm^{-2}$. The composite electrolytes can be designed for many electrochemical devices due to the balanced mechanical, thermal and electrochemical properties.

## Acknowledgments

This work was supported in part by the National Science Council under NSC100-2221-E-182-014 and 100-2918-I-182-003.

## References

[1] R. Othman, W.J. Basirun, A.H. Yahaya, A.K. Arof, J. Power Sources 103 (2001) 34.
[2] C.J. Raj, K.B.R. Varma, Electrochim. Acta 56 (2010) 649.
[3] G.M. Wu, S.J. Lin, C.C. Yang, J. Membr. Sci. 275 (2006) 127.
[4] M. Jithunsa, K. Tashiro, S.P. Nunes, S. Chirachanchai, Intl. J. Hydrogen Energy 36 (2011) 10384.
[5] P. Carol, P. Ramakrishnan, B. John, G. Cheruvally, J. Power Sources 196 (2011) 10156.
[6] P.B. Bharbav, V.M. Mohan, A.K. Sharma, V.V.R.N. Rao, Curr. Appl. Phys. (2009) 165.
[7] F.F. Hatta, T.I.T. Kudin, R.H.Y. Subban, A.M.M. Ali, M.K. Harun, M.Z.A. Yahya, Func. Mater. Lett. 2 (2009) 121.
[8] J. Qiao, J. Fu, R. Lin, J. Ma, J. Liu, Polymer 51 (2010) 4850.
[9] N. Fujiwara, M. Yao, Z. Siroma, H. Senoh, T. Ioroi, K. Yasuda, J. Power Sources 196 (2011) 808.
[10] A.M. Bartrom, J.L. Haan, J. Power Sources 214 (2012) 68.
[11] V. Naburchilov, J. Martin, H. Wang, J. Zhang, J. Power Sources 169 (2007) 221.
[12] J. Park, W. Park, J.H. Kim, D. Ryoo, H.S. Kim, Y.U. Jeong, D. Kim, S. Lee, J. Power Sources 196 (2011) 7035.
[13] Y.H. Liao, X.P. Li, C.H. Fu, R. Xu, M.M. Rao, L. Zhou, S.J. Hu, W.S. Li, J. Power Sources 196 (2011) 6723.
[14] N.H. Idris, M.M. Rahman, J.Z. Wang, H.K. Liu, J. Power Sources 201 (2012) 294.
[15] G. Merle, S.S. Hosseiny, M. Wessling, K. Nijmeijer, J. Membr. Sci. 409 (2012) 191.
[16] P. Raghavan, J. Manuel, X. Zhao, D. Kim, J. Ahn, C. Nah, J. Power Sources 196 (2011) 6742.
[17] R. Prasanth, V. Aravindan, M. Srinivasan, J. Power Sources 202 (2012) 299.
[18] G. Sasikumar, J.W. Ihm, H. Ryu, Electrochim. Acta 50 (2004) 598.
[19] G.M. Wu, Y.T. Shyng, Composites Part A 35 (2004) 1291.
[20] M. Ueno, N. Imanishi, K. Hanai, T. Kobayashi, A. Hirano, O. Yamamoto, Y. Takeda, J. Power Sources 196 (2011) 4756.
[21] A.C.Y. Wong, F. Lam, Polym. Test. 21 (2002) 691.
[22] Z. Cai, C. Hou, J. Power Sources 196 (2011) 10731.